Proceedings of the 1998 U.S. DOE Hydrogen Program Review

NREL/CP-570-25315

CARBON NANOTUBE MATERIALS FOR HYDROGEN STORAGE

A.C. Dillon, P.A. Parilla, K.M. Jones, G. Riker, and M.J. Heben
National Renewable Energy Laboratory
Golden, CO 80401-3393

Abstract

Carbon single-wall nanotubes (SWNTs) are essentially elongated pores of molecular dimensions and are capable of adsorbing hydrogen at relatively high temperatures and low pressures. This behavior is unique to these materials and indicates that SWNTs are the ideal building block for constructing safe, efficient, and high energy density adsorbents for hydrogen storage applications. In past work we developed methods for preparing and opening SWNTs, discovered the unique adsorption properties of these new materials, confirmed that hydrogen is stabilized by physical rather than chemical interactions, measured the strength of interaction to be ~ 5 times higher than for adsorption on planar graphite, and performed infrared absorption spectroscopy to determine the chemical nature of the surface terminations before, during, and after oxidation. This year we have made significant advances in synthesis and characterization of SWNT materials so that we can now prepare gram quantities of high-purity SWNT samples and measure and control the diameter distribution of the tubes by varying key parameters during synthesis. We have also developed methods which purify nanotubes and cut nanotubes into shorter segments. These capabilities provide a means for opening the (10,10) tubes which were unreactive to the oxidation methods that successfully opened (9,9) tubes, and offer a path towards organizing nanotube segments to enable high volumetric hydrogen storage densities. We also performed temperature programmed desorption spectroscopy on high purity carbon nanotube material obtained from our collaborator Prof. Patrick Bernier and finished construction of a high precision Seivert's apparatus which will allow the hydrogen pressure- temperature-composition phase diagrams to be evaluated for SWNT materials.

Statement of the Problem / Relevance of the Work

Background

With the 1990 Clean Air Act and the 1992 Energy Policy Act, the United States recognized the need for a long term transition strategy to cleaner transportation fuels [1]. This realization comes while the U.S. continues to increase petroleum imports beyond 50% of total oil consumption, with nearly 50% of the total oil consumed being used in the transportation sector [2]. Because of the potential for tremendous adverse environmental, economic, and national security impacts, fossil fuels must be replaced with pollution-free fuels derived from renewable resources. Hydrogen is an ideal candidate as it is available from domestic renewable resources and usable without pollution. It could, therefore, provide the long-term solution to the problems created by the Nation's dependence on fossil fuel.

Interest in hydrogen as a fuel has grown dramatically since 1990, and many advances in hydrogen production and utilization technologies have been made. However, hydrogen storage technology must be significantly advanced in performance and cost effectiveness if the U.S. is to establish a hydrogen based transportation system. As described in the U.S. DOE Hydrogen Program Plan for FY 1993 - FY 1997, compact and lightweight hydrogen storage systems for transportation do not presently exist.

Hydrogen provides more energy than either gasoline or natural gas on a weight basis. It is only when the weight, volume, and round-trip energy costs of the entire fuel storage system and charging/discharging cycle is considered that hydrogen's drawbacks become apparent. New approaches enabling more compact, lightweight, and energy efficient hydrogen storage are required in order for the wide-spread use of hydrogen powered vehicles to become a reality.

Research and development geared towards implementation of a national hydrogen energy economy has many indirect economic benefits. With almost 600 million vehicles in the world in 1992 - double the number in 1973 - the conflict between energy requirements, power generation, and environmental concerns is felt on a world-wide basis [3]. Thus, in addition to providing domestic energy alternatives, investment in hydrogen energy research will result in opportunities for U.S. technologies in over-seas markets.

Currently Available Hydrogen Storage Technologies

Hydrogen can be made available on-board vehicles in containers of compressed or liquefied H_2, in metal hydrides, or by gas-on-solid adsorption. Hydrogen can also be generated on-board by reaction or decomposition of a hydrogen containing molecular species [4]. Although each method possesses desirable characteristics, no approach satisfies all of the efficiency, size, weight, cost and safety requirements for transportation or utility use. The D.O.E. energy density goals for vehicular hydrogen storage call for systems with 6.5 wt % H_2 and 62 kg H_2/m^3 to provide a 350 mile range in a fuel cell powered vehicle. This requirement amounts to the storage of ~2.9 kg of H_2 in the weight and volume occupied by a conventional gasoline tank. These storage density goals will only be met with significant advances in the capabilities of hydrogen storage technologies.

Gas-on-solid adsorption is an inherently safe and potentially high energy density hydrogen storage method which should be more energy efficient than either chemical or metal hydrides, and compressed gas storage. Consequently, the hydrogen storage properties of high-surface-area "activated" carbons have been extensively studied [5-7]. However, activated carbons are

ineffective in hydrogen storage systems because only a small fraction of the pores in the typically wide pore-size distribution are small enough to interact strongly with gas phase hydrogen molecules.

Technical Approach and Summary of Past Work

The gas adsorption performance of a porous solid is maximized when all pores are not larger than a few molecular diameters [8]. Under these conditions the potential fields from the walls of the so-called micropores overlap to produce a stronger interaction than would be possible for adsorption on a semi-infinite plane. At sufficiently low temperatures, where the escaping tendency of the gas is much less than the adsorption potential, the entire micropore may be filled with a condensed adsorbate phase. For the case of hydrogen, with a van der Waals diameter of 2.89 Å [9] pores would be required to be smaller than ~40 Å to access this nanocapillary filling regime. Sufficiently small pores would exhibit an adsorption potential strong enough to localize H_2 at relatively high temperatures. Ideally, the entire porous volume of an adsorbent would be of the microporous variety, and the volume and mass of the adsorbent skeleton would be the minimum necessary to develop the adsorption potential and provide sufficient thermal conductivity for management of heat fluxes associated with adsorption and desorption.

We have been working on the idea that aligned and self-assembled single wall carbon nanotubes could serve as ideal hydrogen adsorbents since 1993. The concept was motivated by theoretical calculations which suggested [10] that adsorption forces for polarizable molecules within SWNTs would be stronger than for adsorption on ordinary graphite. Thus, high H_2 storage capacities could be achieved at relatively high temperatures and low pressures as compared to adsorption on activated carbons.

In the Proceedings of the 1994 Hydrogen Program Review, we presented microbalance data which demonstrated gravimetric hydrogen storage densities of up to 8.4 wt% at 82 K and 570 torr on samples containing carbon nanotubes. This substantial uptake at low hydrogen pressures demonstrated the strong interaction between hydrogen and these materials, consistent with higher heats of adsorption than can be found with activated carbons.

In the 1995 Hydrogen Program Review Proceedings, we presented the results of our temperature programmed desorption (TPD) studies which showed significant H_2 adsorption near room temperatures. The adsorption energies on nanotube materials were estimated to be a factor of 2-3 times higher than the maximum that has been observed for hydrogen adsorption on conventional activated carbons. To our knowledge, these are the first results which demonstrate the existence of stable adsorbed hydrogen *on any type of carbon at temperatures in excess of 285 K*. We also analyzed the nanotube production yields versus rod translation rate in the electric arc.

In 1996 we performed a detailed comparative investigation of the hydrogen adsorption properties of SWNT materials, activated carbon, and exfoliated graphite. We also determined that the cobalt nanoparticles present in the arc-generated soots do not play a role in the observed hydrogen uptake. We determined the amount of hydrogen which is stable at near room temperatures on a SWNT basis is ~ 10 wt%, and found that an initial heating in vacuum is essential for producing high temperature hydrogen adsorption. Further experiments suggested that SWNTs are selectively opened by oxidation during this heating, and that H_2O is more selective in oxidation than O_2 due to hydrogen termination of dangling bonds at the edges of opened nanotubes. Purposeful oxidation in H_2O resulted in hydrogen storage capacities which were improved by more than a factor of three. We also correlated the measured nanotube densities produced by specific synthesis rod translation rates during arc-discharge with hydrogen storage capacities determined by TPD. Finally, we utilized NREL's High Flux Solar Furnace to form nanotubes by a new and potentially less expensive route for the first time.

In 1997 we confirmed that H_2 is stabilized by purely physical - rather than chemical - binding. The desorption of hydrogen was found to fit 1st order desorption kinetics as expected for physisorbed H_2, and the activation energy for desorption was measured to be 19.6 kJ/mol. This value is approximately five times higher than the value expected for desorption of H_2 from planar graphite and demonstrates that SWNT soots can provide very stable environments for H_2 binding. We also employed diffuse reflectance Fourier transform infrared (DRFTIR) spectroscopy to determine the concentrations and identities of chemisorbed species bound to the carbon surface as a function of temperature, and determined that "self-oxidation" allows high-temperature adsorption of hydrogen to occur in (9,9) SWNT materials. We also began synthesizing SWNT materials in much higher yield than is currently possible with arc-discharge by using a laser vaporization process, and determined that the (10,10) tubes predominantly made by this method could not be activated towards high-temperature H_2 physisorption by the same oxidative methods that were found to be effective for tubes produced by arc-discharge.

This year we have made significant advances in synthesis and characterization of SWNT materials so that we can now prepare gram quantities of high-purity SWNT samples and measure and control the diameter distribution of the tubes by varying key parameters during synthesis. We have also developed methods which purify nanotubes and cut nanotubes into shorter segments. These capabilities provide a means for opening the (10,10) tubes which were unreactive to the oxidation methods that successfully opened (9,9) tubes, and offer a path towards organizing nanotube segments to enable high volumetric hydrogen storage densities. We also performed temperature programmed desorption spectroscopy on high purity carbon nanotube material obtained from our collaborator Prof. Patrick Bernier, and finished construction of a high precision Seivert's apparatus which will allow the hydrogen pressure- temperature-composition phase diagrams to be evaluated for SWNT materials.

Experimental

Pulsed and Continuous Wave Laser Synthesis of SWNTs

Powdered graphite (particle size 4μ) doped with 0.6 atomic % each of Co and Ni powder (particle size 1 μ) was uniformly combined with polyethylene glycol, M_n ~ 3400, (PEG) in a 50 wt% ratio. Four grams of the final mixture was pressed in a 1 inch dye with a Carver hydraulic press at 10,000 pounds for 3 min. The targets thus obtained were slowly heated in argon between 200-1000 °C over 8 hrs. and maintained at 1000 C for an additional 4 hrs. Above ~400 C the PEG was observed to completely evolve. The resulting porous cobalt-nickel/graphite targets had expanded ~ 25% and had a density of ~0.3 g/cm^2. Targets with 30 and 40 wt % PEG as well as dense targets containing only the cobalt-nickel/graphite mixture were also fabricated.

During the syntheses, the targets were supported with a tantalum holder in a 1 1/2 inch quartz tube which could be enclosed by a circular single-zone furnace. Prior to laser irradiation the quartz tube was purge-cycled three times between 1 and 750 Torr Ar over 20 min. while the target was baked with an infrared lamp. During the experiments the chamber pressure was maintained at 500 Torr with Ar flowing at 50 sccm. A Control Q-switched Nd:Yag (1064 nm) laser beam was directed at normal incidence by a scanning mirror and focused to ~ 0.86 mm^2. The beam was rastered in a rectangular pattern at frequencies of 0.01 and 1 Hz in the x and y directions, respectively. The laser power could be easily monitored at various points in the experiments with a Scientech AC50HD calorimeter head.

Targets prepared with 50% PEG were shown to be the most efficient for the room temperature production of SWNTs. The following detailed analysis was thus performed using only these highly porous targets. Pulsed laser experiments were conducted at pulse repetition rates

of 3, 6, 10 and 24 kHz. The operating characteristics of the laser are such that the pulse frequency, pulse width, and energy per pulse are all interdependent. Table 1 lists the corresponding values for these experiments as well as the calculated peak power and measured average power. Continuous wave (c.w.) experiments with average powers corresponding to the respective average powers of the pulsed runs and a maximum average power experiment of 30 W were also performed. The laser radiation exposures were 30 min. However, in each of the experiments the appearance of cones or spires on the target surface led to a dramatic drop-off in the target etch rate consistent with previous laser sputtering reports of HOPG[11]. For all of the laser runs, carbon soot was collected on the quartz tube directly above the target holder. For the c.w. and both the 24 and the 25.5 kHz pulsed experiments a "web"-like material spanned the tube walls directly behind the target holder. Following each experiment, the soot and web components were collected separately for TEM analysis.

Pulse Frequency (kHz)	Pulse Width (nsec)	Energy Density per Pulse (J/cm2)	Peak Power (kW)	Average Power (W)
3	~175	0.62	~30	16
6	~250	0.39	~13	20
10	~300	0.28	~8	24
24	~575	0.12	~2	25.5

Table 1: Pulsed laser operating characteristics of the Nd-Yag laser for the experiments. Pulse widths and peak power are estimates based on manufacturer's specifications.

A Molectron MY35 Nd:Yag laser was used to produce large quantities of material. The pulse width and repetition rate were held constant for most of these synthesis runs at values of ~100 ns and 10 Hz, respectively. When Q-switching was employed the pulse width was compressed to ~ 10 ns. A maximum energy of approximately 850 mJ/ pulse could be obtained. The laser light was focused to a spot that ranged in size from 1-10 mm^2, and rastered on the target in the same manner as reported above. Dense targets were fabricated from powdered graphite (particle size 4μ) doped with 0.6 atomic % each of Co and Ni powder (particle size 1 μ) by pressing four grams of the mixture with a Carver hydraulic press at 10,000 pounds for 3 min. in a 1 inch dye. Porous targets were ablated, rather than vaporized, at these high energy densities and were only cursorily investigated. The target temperature could be controlled from room temperature to 1200 °C with a three-zone clam-shell furnace. The pressure and flow rate of the inert ambient could be independently controlled. Most runs were performed at 500 Torr in the presence of a 100 sccm flow of Ar gas.

Purification of Laser-generated SWNTs

Approximately 0.1g of laser-generated SWNT material was refluxed in 28 ml of 2.6 M nitric acid for 25 hrs. at 120° C. Upon cooling the solution was filtered with a 0.2μ Anotec alumina filter. The collected material consisted of a black carbon paste and was resuspended in 56 ml of 2.6 M HNO_3 and sonicated for 1 hr. This new solution was again filtered, and the precipitate was rinsed with d.i. water and allowed to dry. The final collected carbon material had a paper-like consistency. Following both filtrations the nitric acid filtrate was brown in color.

Cutting of Laser-generated SWNTs

Approximately 50 mg of the laser-generated SWNT material was sonicated for 24 hrs in the following solutions: concentrated H_2SO_4, HCl, Aqua Regia (4:1 HCl:HNO_3), 3:1 H_2SO_4:HNO_3, 5:18:1 HCl:H_2SO_4:HNO_3, and 5% Bromine and Iodine in methanol. The solutions were filtered

with 0.2μ Anotec alumina filters. In each case a black carbon past-like material was collected for TEM analysis.

Transmission Electron Microscopy (TEM)

Samples were prepared for TEM by suspending 0.2 mg in 10 ml of acetone. The solutions were sonicated for 5 min., and 6 drops were placed on Ted Pella Ultra-thin Carbon Type-A 400 mesh grids. TEM images were obtained on a Phillips CM-30 TEM/STEM operating at 200 kV with a 50 μm objective aperture for improved contrast. The images were recorded on a 1024 x 1024 CCD camera

For the quantitation of SWNT contents in the laser-generated materials three grids of each sample were prepared. Three images of each grid were then taken at random different spots on the grid with a magnification of 17k for a total of nine images of each sample. An additional high resolution image displaying the lattice patterns of the individual SWNTs was taken at a magnification of 160k. The two-dimensional spatial areas of the cobalt particles, amorphous carbon / nano-crystalline graphite and SWNTs observed in the TEM images were obtained using the NIH Image graphical analysis software package. Measurements of SWNT, amorphous carbon / nanocrystalline graphite and cobalt particle densities were then quantified as a statistical average of the nine images of each sample.

For the cutting and purification studies each sample was surveyed for ~45 minutes, and ~ 5 images were recorded between 4.4k and 160k to ensure a true representation of the material.

Raman Spectroscopy

Raman spectra were obtained from pure samples of collected carbon soots. The Raman backscattering was excited using 50 mW of the 488 nm wavelength of an Ar ion laser. The scattered light was analyzed in a Jobin Yvon 270M spectrometer with a 1200 groves/nm grating equipped with a liquid-nitrogen cooled Spectrum One CCD and a holographic notch filter. A Nikon 55 mm camera lens was employed to focus the beam on the sample to a spot approximately 0.25 mm^2. Light polarized both perpendicular and parallel to the scattering plane was collected. Spectra were recorded with the laser at normal incident to the sample and with an integration time of 10-30 min. A resolution of ~ 0.6 nm (2-6 cm^{-1}) was measured with the 546.07 nm line of an Oriel Hg(Ar) spectral calibration lamp.

Temperature Programmed Desorption

Details of the ultra high vacuum (UHV) chamber employed for the TPD studies have been reported previously. Briefly, the sample is mounted at the bottom of a liquid nitrogen cooled cryostat, and a mass spectrometer provides for line-of-site detection of desorbing species. An ion gauge and capacitance manometer are employed to monitor pressure. Gas exposure is controlled with a variable conductance leak valve. Isolation gate valves separate the sample compartment during high-pressure gas exposures.

Carbon samples weighing ~1 mg were placed in a packet formed from 25 μm thick platinum foil. Pin holes in the foil enabled gas diffusion into and out of the packet. The packet could be cooled to ~90 K by the liquid nitrogen cryostat, and resistively heated with a programmable power supply. The sample temperature was measured with a thin thermocouple spot-welded to the platinum packet. The samples were heated in vacuum at 1 K/s to 970 K prior to TPD studies. Hydrogen (99.999% purity) exposures between 300-600 Torr at room temperature were employed to elucidate the H_2 adsorption properties of the samples. The samples were cooled to ~ 130 K prior to the evacuation of the hydrogen gas.

Results and Discussion

Optimization of Laser Synthesis of SWNTs

Pulsed and continuous wave laser light was directed on porous cobalt-nickel / graphite targets at room temperature and the generation of SWNTs was examined. In all of the laser experiments the condensed carbon material took the form of either a rubbery soot or a very fine web-like material. Both types of materials were collected and analyzed with TEM. These materials were composed of various fractions of amorphous carbon / nano-crystalline graphite, cobalt/nickel nano-particles and single-wall carbon nanotubes. No multi-walled carbon nanotubes or large graphitic fragments were observed. Within any given experiment, the web portion of the collected material had a much higher SWNT density than that of the soot. The web component was not observed for experiments in which SWNTs were found only in low yields in the soot. The fraction of cobalt/nickel nano-particles remained essentially constant at ~ 15% in both the web and soot materials in all of the experiments. The quantity of SWNTs produced relative to the amount of amorphous carbon or nano-crystalline graphite varied dramatically with the character of the target and laser operating parameters.

Room temperature c.w. (30 W) laser production of SWNTs was shown to be most efficient for porous targets. Dense targets, prepared without any binder, did not result in the production of SWNTs for either pulsed experiments between 3-25.5 kHz or c.w. experiments between 16-30 W. Previous studies indicated that SWNT laser-vaporization yields increased with increasing target temperature up to 1200 °C[12]. However, a target temperature of 1000 °C did not increase the SWNT production yield in comparison to room temperature, 30 W c.w. runs.

Figure 1 displays SWNT densities in a) collected web and b) collected soot components for both laser techniques with irradiation of 50% porous targets. The c.w. experiments were performed at the average power which was measured for each of the pulsed experiments. Figure 1 demonstrates that for both c.w. and pulsed operation a linear increase in the fraction of SWNTs is observed for increasing average laser power. Note that no web component of material was visible in the chamber for the slower pulsed runs of 3 and 6 kHz (0.62 and 0.39 J/cm2),. In fact, no SWNTs were observed for the 3 kHz (16 W) experiment, and the soot material collected for the 6 kHz (20 W) experiment contained only ~4% SWNTs.

The SWNT densities in the pulsed web material produced in the 10 and 24 kHz experiments closely approach the densities found in the c.w. web material. The SWNTs are much purer in the web components because they easily stick to one another while growing and adhere to the tube walls. Therefore we intuitively expect the SWNT content in the web material to be similar in both c.w. and pulsed experiments. The SWNTs in the soot fractions are not purified in the same manner. Since the web material is a small percentage ($\leq$ 30%) of the total material collected, the data in Figure 1b is more representative of the overall SWNT densities.

Figure 2 a) is a typical TEM image of the soot collected for 6 kHz pulsed laser irradiation. Only a few SWNTs are observed spanning the dense agglomerations of carbon coated cobalt/nickel nano-particles. For comparison, Fig. 2 b) and c) display TEM images of soot collected from the 10 kHz pulsed experiment and the c.w. experiment performed at the corresponding average power of 24 W. The SWNT densities for these operating conditions were ~26% and ~51%, respectively. Finally, the high purity SWNTs (~78%) present in the web component of the material generated with 30 W c.w. laser radiation is shown in Fig. 2 d). Here the material consists primarily of long bundles of SWNTs with only a small amount of amorphous carbon or nano-crystalline graphite found coating the metal particles. Closer inspection of the strands of SWNTs in the images of Fig.

2 revealed bundles of crystalline nanotubes similar to those initially reported for laser synthesis[12, 13].

Clearly the results displayed in Figs. 1 and 2 show that c.w. laser radiation is more effective than pulsed radiation in the production of SWNTs at a given average power. Clues to the underlying reason for this can be found in the experiments using a dense target (without any PEG binder) at room temperature. Here continuous wave experiments (30 W) resulted in a glowing orange spot on the target with no carbon evolution. In contrast, similar conditions for the porous target resulted in the production of a brilliant white light and the evolution of carbon vapor. Apparently the surface temperature never reached the necessary vaporization threshold in the case of the dense target due to the very high thermal conductivity. Pulsed experiments on the dense target at a peak power of ~30 kW (table 1) resulted in the slow removal of particulate matter, but no SWNTs were found. In this case the material was likely removed by ablation rather than vaporization processes. Here, the term "ablation" encompasses a broad scope of processes dealing with a more aggressive ejection of relatively large pieces of the target material. Thus, the energy incident onto the target can be dissipated in either an evaporative or ablative mechanism depending on the target porosity and the time scale in which the energy is delivered. In order to produce SWNTs efficiently it is necessary to remain dominantly in a vaporization regime.

Single-wall carbon nanotubes are highly stable graphitic structures and are therefore favored thermodynamically for formation. It is thus probable that optimal SWNT formation will occur for thermal or near-thermal processes with appropriate nucleation centers. The present study confirms the hypothesis that for the efficient laser-generation of SWNTs, it is necessary to operate primarily in a vaporization regime. In fact, if vaporization mechanisms are exclusively in operation, it may be possible to acquire material which contains only single-wall nanotubes and transition metal nano-particles. We have achieved a dominantly vaporization regime and high yield production of SWNTs at room temperature using a c.w. Nd:Yag laser process.

HNO_3 Purification of SWNTs

Single-wall carbon nanotube materials produced in gram quantities with the Molectron MY35 pulsed Nd:Yag laser vaporization methods were purified by a combination of refluxing and sonicating in nitric acid. Figure 3 a) displays a TEM image of an initial relatively low-quality laser-generated SWNT material. Long bundles of SWNTs are clearly visible in Fig. 3 a), however, the image also reveals a high concentration of amorphous carbon or nanocrystalline graphite as well as cobalt and nickel nanoparticles with diameters between 50-100 nm. Fig. 3 b) displays the same material following the nitric acid purification treatment outlined here. Note that all of the metal nanoparticles and the majority of the other non-nanotube carbon materials have been removed. A slight non-graphitic carbon coating does still remain on the bundles of SWNTs in Fig. 3 b). However, it is likely that the removal of this carbon coating may be achieved by the addition of an HNO_3 sonication step where the acid is decanted away rather than removed by filtration. This purification scheme is simpler and more effective than those previously reported in the literature [14, 15].

Cutting / Opening of Laser-generated SWNTs

The high purity laser generated SWNTs do not enable the adsorption of large quantities of hydrogen as previously anticipated. The 10-15 Å diameter SWNTs produced at high yield by the methods of laser vaporization may be 100's of microns in length. The poor hydrogen uptake by these materials may be attributed to very slow hydrogen diffusion down the long nanotube walls resulting in an effective blockage at the ends of the tubes. Since so few tube ends are present in the laser-generated materials, the overall hydrogen uptake is low. We have explored methods for

cutting these long bundles into segments to produce short opened tubes for effective hydrogen uptake.

The nanotube materials were sonicated in the following solutions known to damage graphitic structures: concentrated H_2SO_4, HCl, Aqua Regia (4:1 HCl:HNO_3), 3:1 H_2SO_4:HNO_3, 5:18:1 HCl:H_2SO_4:HNO_3, and 5% bromine and iodine in methanol. Of these strong oxidizers the concentrated HCl and the mixture containing 5:18:1 HCl:H_2SO_4:HNO_3 were the most effective for the cutting of the long SWNT bundles. Little or no damage was observed to the nanotube structures following treatments with the 5% bromine and iodine in methanol mixtures.

Figure 4 a) displays a TEM image of laser-generated SWNT material sonicated in 5:18:1 HCl:H_2SO_4:HNO_3. Individual nanotubes with lengths between ~0.25 - 1 μ are clearly visible in the image. Figure 4 b) displays a high resolution TEM image of the same initial material following sonication in HCl. A very high density of SWNT ends is apparent. In the untreated samples a clear image of nanotube ends could not be found following hours of TEM analysis. Applying the successful methods of cutting to highly purified SWNT materials and improving methods for the collection of the cut nanotubes should result in a material with very high H_2 adsorption capabilities.

Temperature Programmed Desorption with Electric-Arc Material

High purity carbon nanotube materials which were produced by electric arc at the Universite de Montpellier II by Patrick Bernier's research group were investigated with TPD spectroscopy. Materials produced by the electric-arc method can have diameter distributions different from the diameter distributions found for tubes produced by laser vaporization. Figure 5 shows the TPD spectrum obtained from 1 mg of the Bernier material after the sample was heated in vacuum at 1 K/s to 970 K. The hydrogen exposure was performed at 300 Torr for 10 min. at room temperature. The sample was cooled to ~ 130 K prior to the evacuation of the hydrogen gas.

The TPD signal from the electric arc-material has two peaks in addition to the 145 K peak which is produced by pumping out the hydrogen dose while holding the sample at 130 K. The spectrum differs significantly from those which we typically observe in NREL electric-arc materials. Fig 5. displays peaks at ~205 and 310 K. NREL arc-discharge materials typically display only one peak at ~285K. The Bernier materials are produced with catalytic elements such as lanthanum and yttrium [16] and therefore can contain nanotubes of differing diameters than the tubes we have produced with Ni and Co catalysts in our arc-discharge apparatus. We have not yet performed Raman spectroscopy to characterize the diameter distribution in the Bernier sample, but the TPD spectroscopy suggests a bi-modal distribution of tube diameters in the Bernier sample with one type of tube being larger than (9,9), and the other being smaller. If this interpretation is correct, then improved control over the synthetic process to produce specific diameters will result in the tailoring of SWNTs for adsorption/desorption over specific temperature and pressure conditions.

Production of SWNTs with Specific Diameters

Theoretical calculations predict that the Raman frequencies of the radial breathing modes for SWNTs are diameter dependent. Calculated frequencies include 206, 183, 165 and 150 cm^{-1} for (8,8), (9,9), (10,10) and (11,11) SWNTs where the diameters are 1.08 1.22, 1.35 and 1.49 nm, respectively. Figure 6 displays Raman spectra of the radial breathing modes of SWNT materials formed using the Molectron MY35 Nd:Yag laser. For the top spectrum in Fig. 6 the material was produced using 10 Hz pulses at ~ 800 mJ/pulse at 1000°C. The middle spectrum corresponds to material produced under the same conditions with the target at 1200°C. The spectrum observed for the 1000°C material indicates the production of SWNTs with a fairly wide distribution in size. In the spectrum of the 1200°C material, very little intensity is observed at frequencies > 165 cm^{-1} indicating the production of predominantly larger diameter SWNTs. The bottom spectrum in Fig.

6 is of material produced at 1000°C employing the Q-switched mode of operation with the laser. Here very little intensity is observed for frequencies < 165 cm^{-1} indicating the production of predominantly smaller diameter SWNTs. These results suggest the ability to selectively tune the SWNT diameters by varying the synthesis conditions. These results may prove very crucial to the development of an effective hydrogen storage material as a specific diameter nanotube may be the most effective for the high uptake of hydrogen.

Seivert Apparatus for Pressure-Composition-Temperature Measurements

As noted previously [17], the behavior of SWNTs in real-world hydrogen storage applications will be governed by their charge/discharge capabilities while in the presence of over-pressures of hydrogen. Our work has been focused on the TPD behavior of hydrogen desorbing from these materials into an UHV environment since the TPD technique is very sensitive, and only small quantities of SWNTs could be synthesized until recently. Since we are now able to fabricate gram quantities, we are in a position to evaluate the pressure-composition-temperature phase diagrams for H_2 interacting with carbon nanotubes.

A Sievert apparatus has been constructed to measure the absorption of hydrogen in nanotubes as a function of pressure, temperature, and nanotube processing. Its operating principle is based on introducing a known amount of a gas into a known volume containing an absorption sample and measuring the pressure. By assuming an equation of state (usually the ideal gas law), the amount of absorbed gas can be calculated. To accurately determine the absorbed amount requires measuring the temperature, volume, and pressure of both the reference and sample chambers to high accuracy. Careful calibration procedures must be observed to determine the reference and sample chamber volumes. There are numerous subtle considerations, such as the volume displaced by the sample itself and the effect of temperature and pressure on the volumes, that must be factored into the calibration and absorption calculations.

The apparatus built at NREL consists of several components and the block diagram of the Sievert apparatus is given in Figure 7. The maximum pressure rating for the setup is 5000 psi; however, our maximum pressure source is currently 2500 psi. There is a vacuum system to initially evacuate all volumes of the system as well as to assist in the initial degassing of the sample. The experiment can then proceed with the pressures being recorded and pneumatic valves operating under computer control. At the present time, the apparatus operates at room temperature; however, we are working on extending the operating temperature range to 75 - 775 K. The system currently is undergoing verification tests and trial runs. It is expected that we will be able to readily detect the absorption of ~10^{-3} moles of gas which corresponds to 0.2 wt. % of hydrogen in a 1 gram sample of nanotubes.

Conclusions / Future Work

This year we have made significant advances in the synthesis and characterization of SWNT materials so that their potential may be realized in hydrogen storage applications. We can now prepare gram quantities of high-purity SWNT samples and measure and control the diameter distribution of the tubes by varying key parameters during synthesis. We have also developed methods which purify nanotubes and cut nanotubes into shorter segments. These capabilities provide a means for opening the (10,10) tubes which were unreactive to the oxidation methods that successfully opened (9,9) tubes, and offer a path towards organizing nanotube segments to enable high volumetric hydrogen storage densities. Further work in this area will be focused on improving yield and selectivity of the purifying and cutting procedures. We also performed temperature programmed desorption spectroscopy on high purity carbon nanotubes material obtained from our collaborator Prof. Patrick Bernier. The difference in the hydrogen storage capabilities of these materials will be investigated in more detail in the future to allow further

control and improvement in the H_2 storage behavior of SWNT materials. We have finished construction of a high precision Seivert's apparatus which will allow the hydrogen pressure-temperature-composition phase diagrams to be evaluated for SWNT materials, and detailed work in this area will be a main focus during the upcoming year.

References

1. Cannon, J.S., *Harnessing Hydrogen.* 1995, New York: INFORM, Inc.

2. N.E.S., *National Energy Strategy.* 1991/1992. .

3. Flavin, C. and N. Lessen, *Power Surge.* 1994, New York: W.W. Norton & Co.

4. Dillon, A.C., *et al. Carbon Nanotube Materials for Hydrogen Storage.* in *Proceedings of the U.S. DOE Hydrogen Program Review.* 1995. Coral Gables, FL:

5. Carpetis, C. and W. Peschka, *A Study of Hydrogen Storage by Use of Cryoadsorbents.* Int. J. Hydrogen Energy, 1980. **5**: p. 539-554.

6. Schwarz, J.A. *Activated Carbon Based Storage System.* in *Proceedings of the 1993 DOE/NREL Hydrogen Program Review.* 1993. Cocoa Beach, FL.:

7. Schwarz, J.A. *Modification Assisted Cold Storage (MACS).* in *contract report to Brookhaven National Laboratories, contract # 186193-S.* 1.

8. Gregg, S.J. and K.S.W. Sing, *Adsorption, Surface Area and Porosity.* 2nd. ed. 1982, London: Academic Press.

9. Breck, D.W., *Zeolite Molecular Sieves: Structure, Chemistry and Use.* 1974, New York: Wiley.

10. Pederson, M.R. and J.Q. Broughton, *Nanocapillarity in Fullerene Tubules.* Physical Review Letters, 1992. **69**: p. 2689.

11. Krajnovich, D.J., J.E. Vazquez, and R.J. Savoy, *Impurity-Driven Cone Formation During Laser Sputtering of Graphite.* Science, 1993. **259**: p. 1590.

12. A.Thess, *et al., Cryastalline Ropes of Metallic Carbon Nanotubes.* Science, 1996. **273**: p. 483-487.

13. Guo, T., *et al., Catalytic growth of single-walled nanotubes by laser vaporization.* Chem. Phys. Lett., 1995. **243**: p. 49-54.

14. Bandow, S., *et al., Purification of single-wall carbon nanotubes by microfiltration.* Journal of Physical Chemistry B, 1998. **101**(44): p. 8839-42.

15. Jie Liu, *et al., Fullerene Pipes and Capsules.* Nature, 1997. **(in the press)**.

16. Journet, C., *et al., Large-scale production of single-walled carbon nanotubes by the electric-arc technique.* Nature (London), 1997. **388**(6644): p. 756-758.

17. Dillon, A.C., *et al., Storage of Hydrogen in Single-Wall Carbon Nanotubes.* Nature, 1997. **386**: p. 377-379.

Acknowledgments

We are grateful for the assistance of J.D. Perkins and M.D. Landry for assistance with experimental set-up, and the research group of P. Bernier for providing SWNT samples prepared by electric-arc.

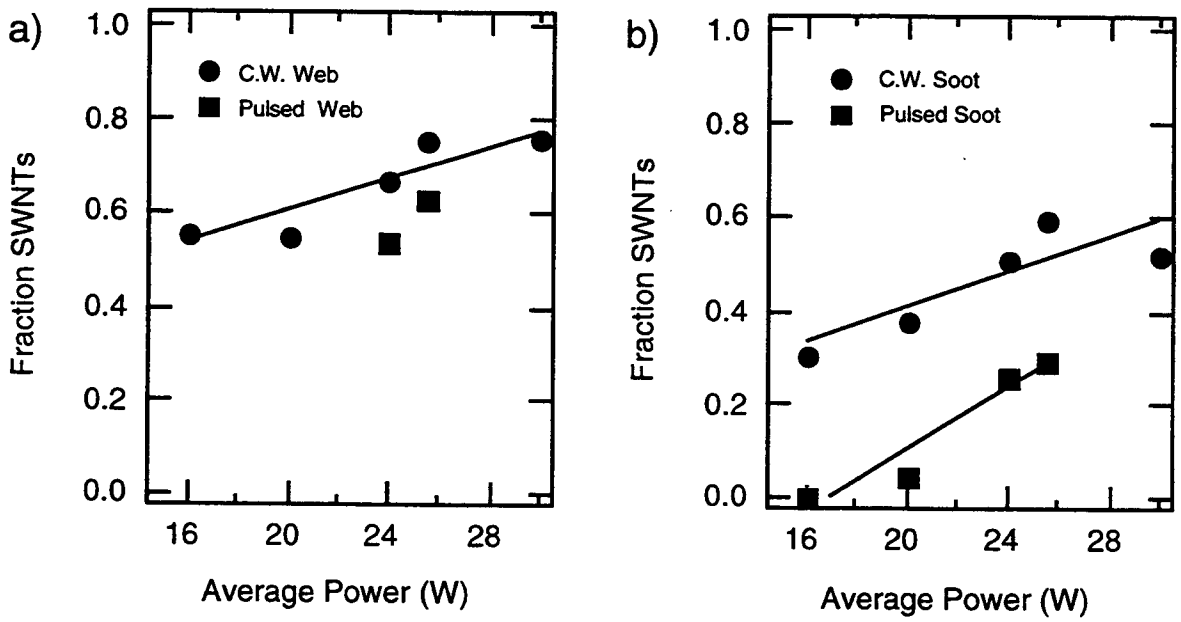

Figure 1: SWNT densities observed for pulsed and c.w. laser production in a) collected web and b) collected soot components. The c.w. experiments were performed at the average power which was measured for each of the 3, 6, 10 and 24 kHz pulsed experiments (see Table 1). SWNT fractions are given versus average laser power for both c.w. and pulsed modes of operation.

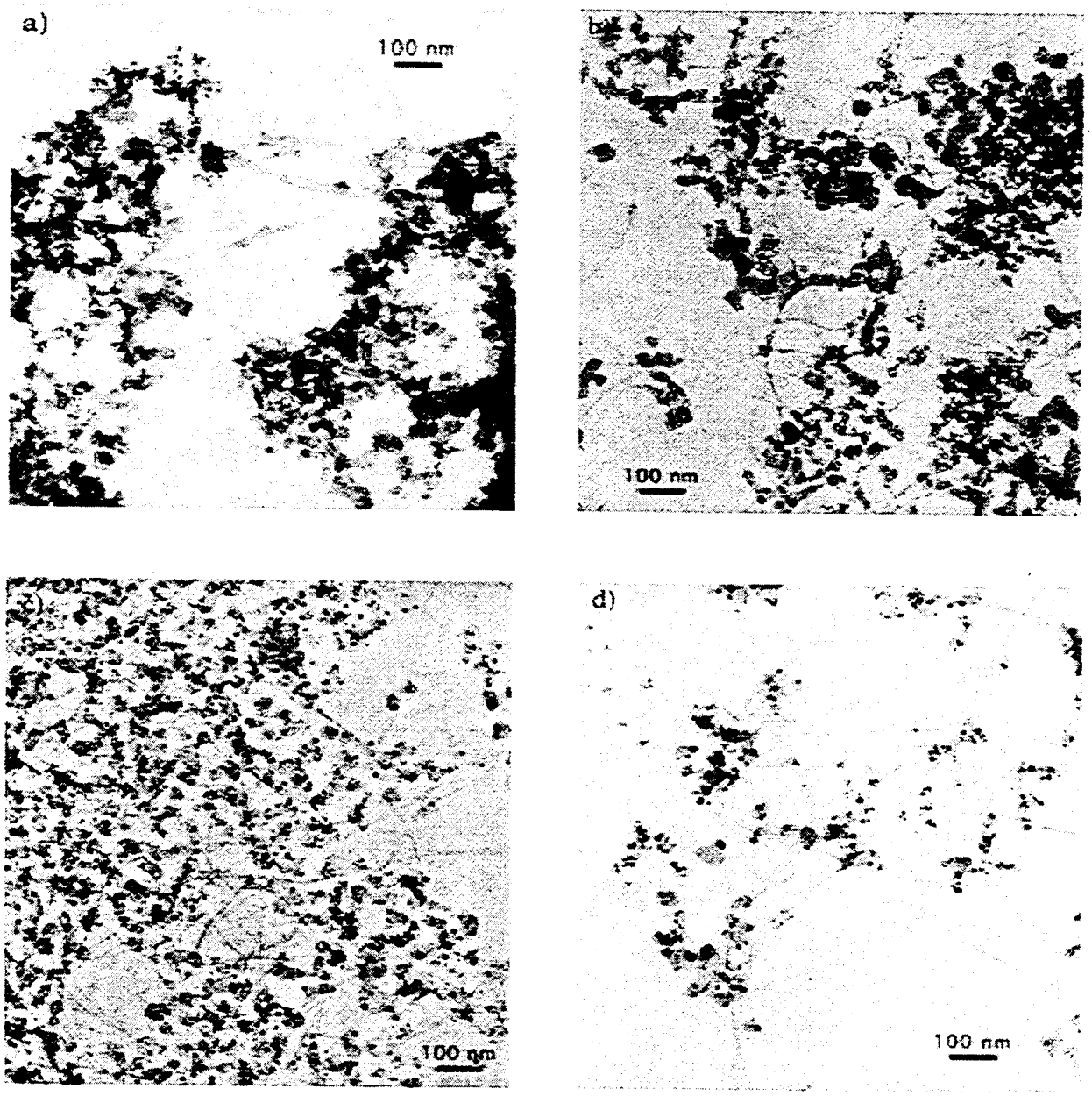

Figure 2: Characteristic TEM images of the material collected following laser irradiation of porous nickel-cobalt /graphite targets. a) soot produced by 6 kHz pulses, ~4% SWNTs, b) soot produced by 10 kHz pulses, ~26% SWNTs, c) soot produced by 24 W c.w. laser light, ~51% SWNTs, and d) web produced by 30W c.w. laser light, ~78% SWNTs.

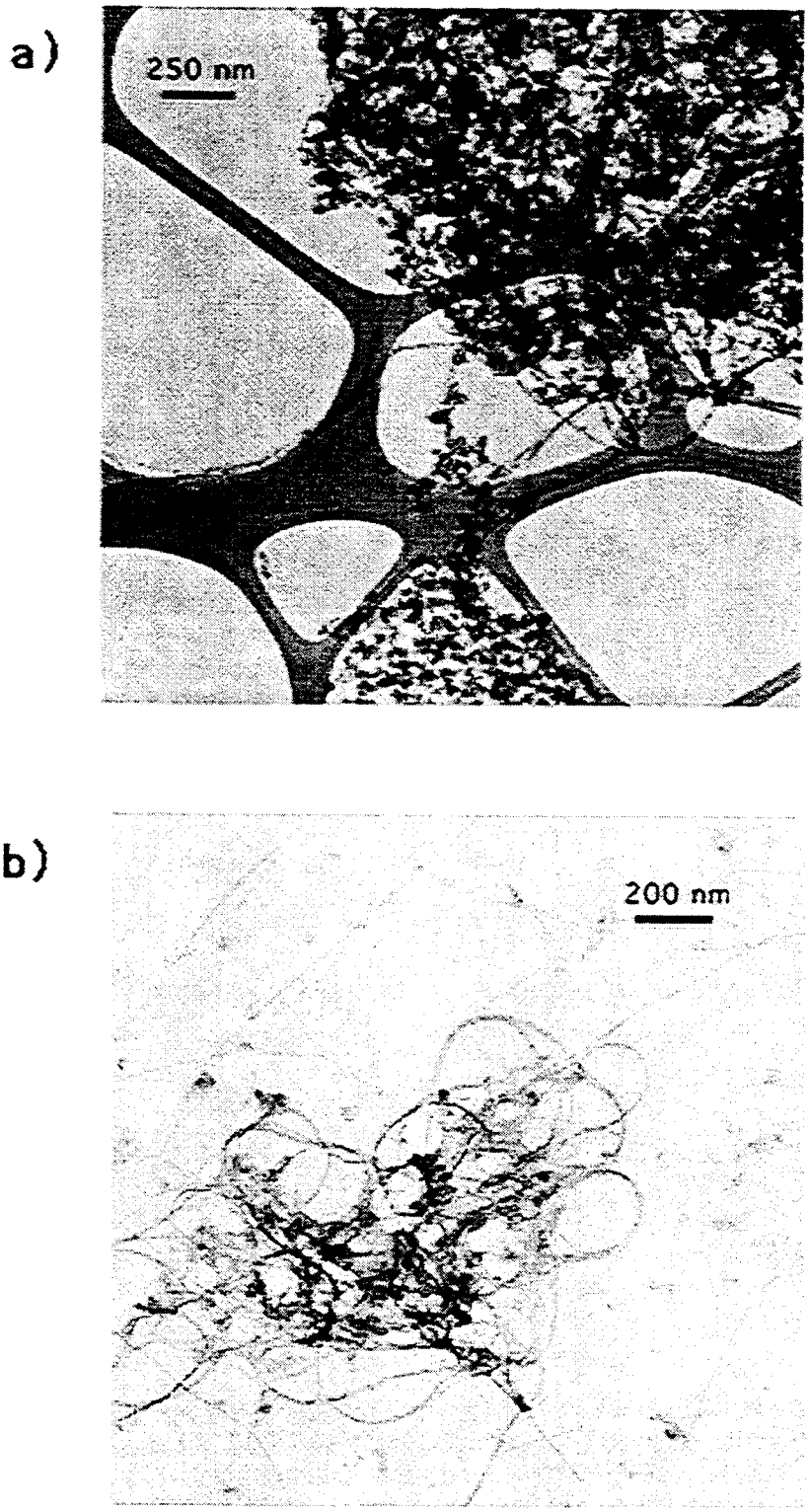

Figure 3: TEM images of a) initial relatively low quality pulsed laser generated SWNT material and b) the same material following nitric acid purification.

a)

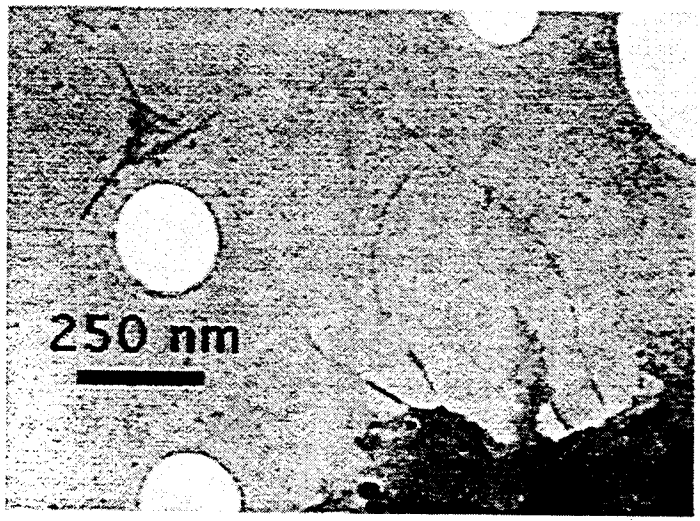

b)

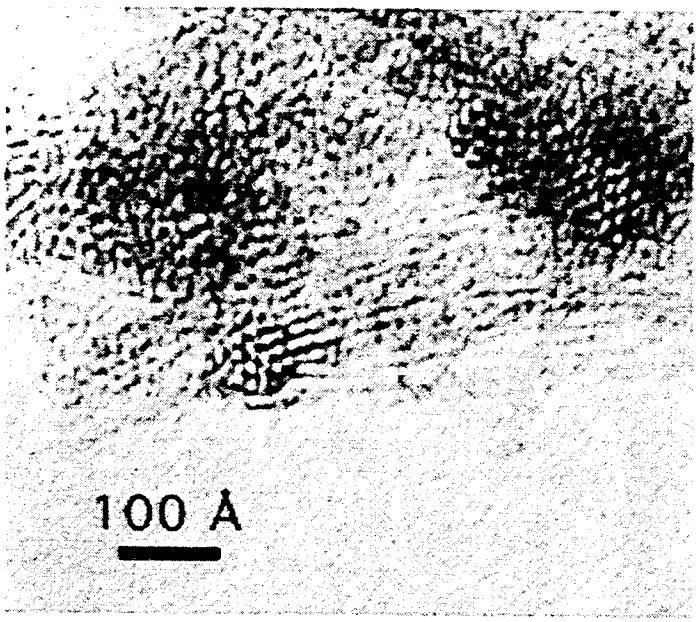

Figure 4: TEM images of laser produced SWNT materials following a) sonication in 5:18:1 $HCl:H_2SO_4:HNO_3$ where SWNTs with ~0.25-1μ lengths are observed and b) sonication in HCl revealing a high density of nanotube ends.

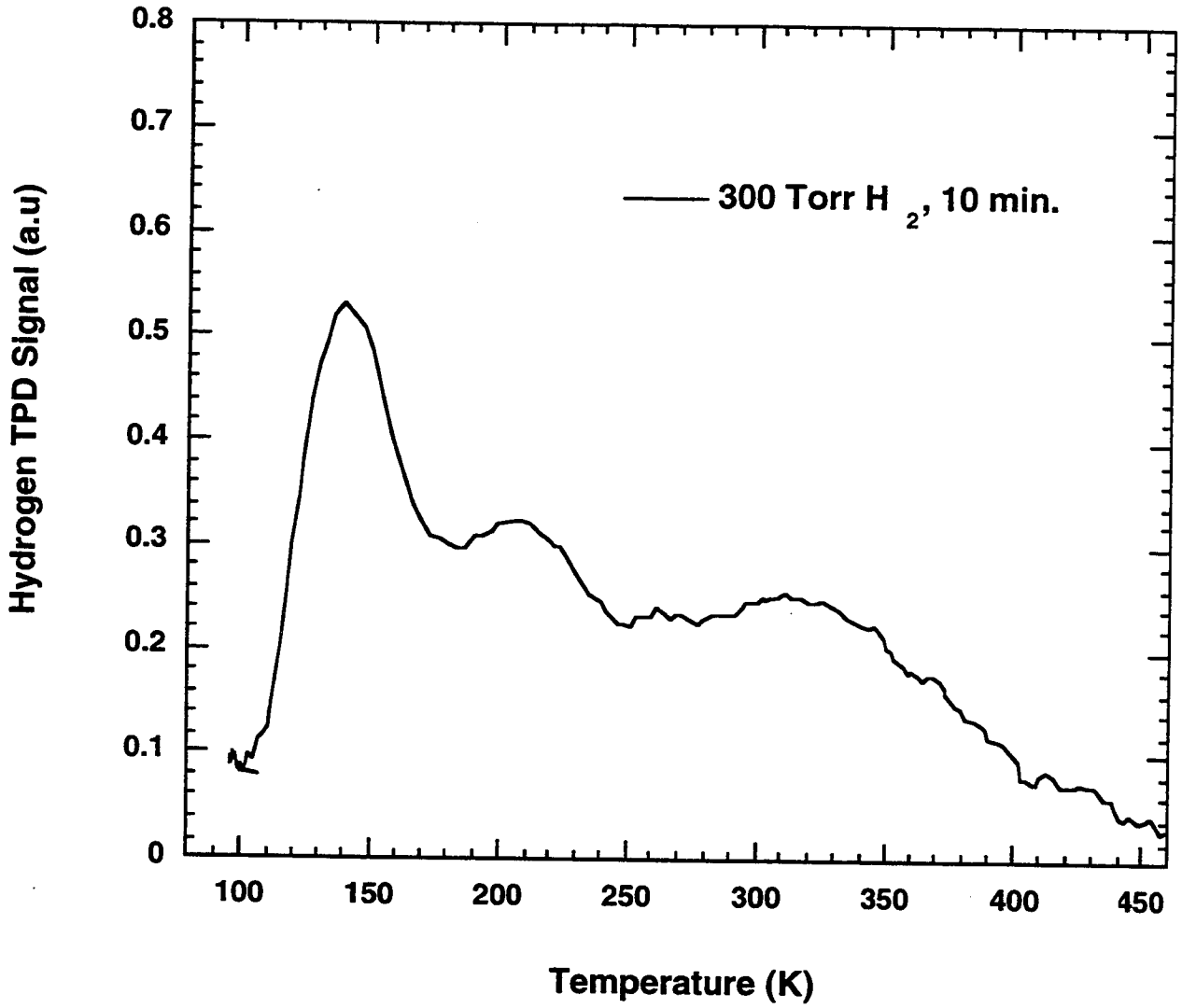

Figure 5: Temperature programmed desorption spectrum of material produced by electric-arc and supplied by P. Bernier.

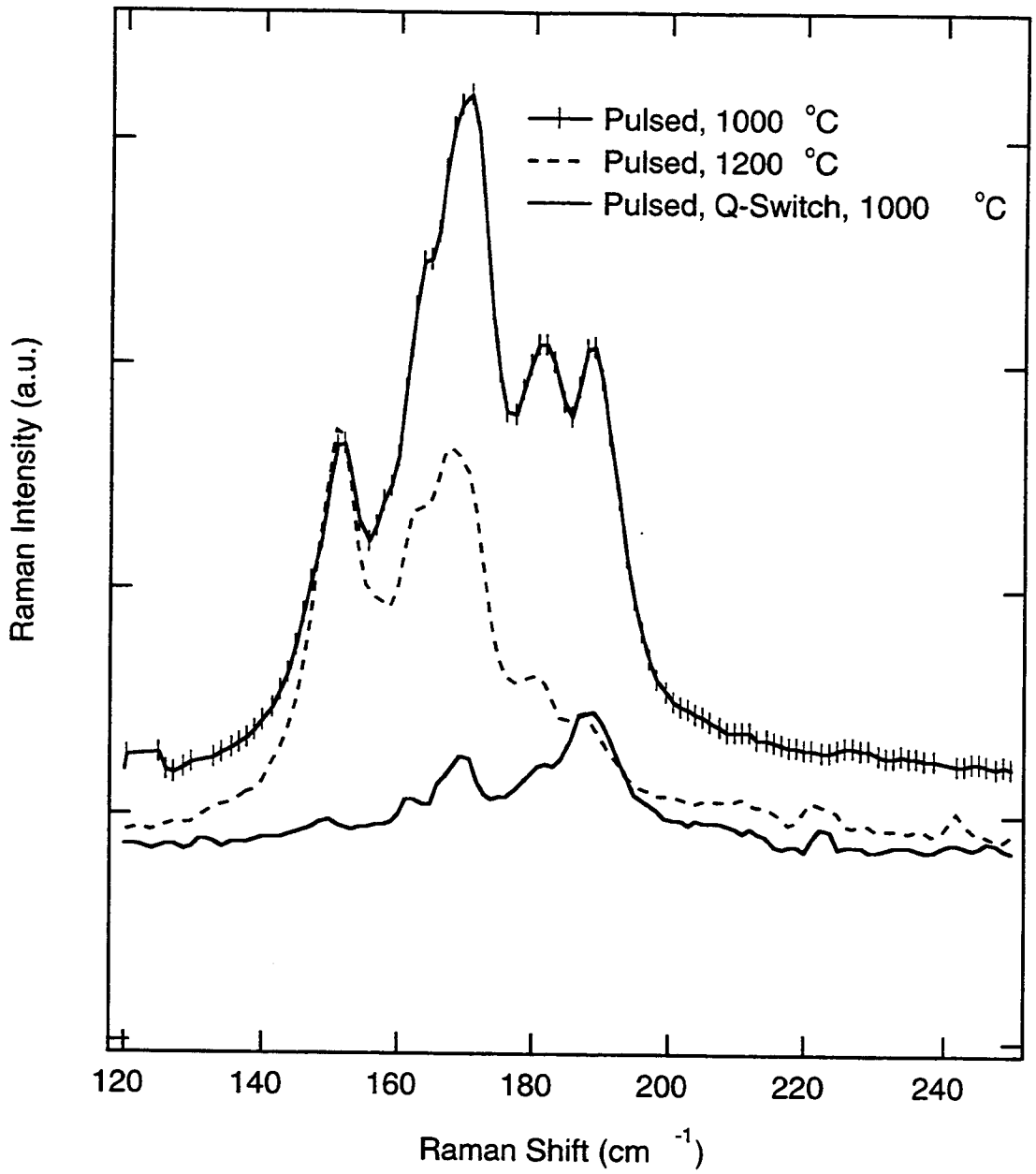

Figure 6: Raman spectra in the region of the radial breathing mode for various laser generated SWNT materials indicating the ability to produce nanotubes with differing diameters by varying synthesis parameters.

Sievert Apparatus

for measurement of hydrogen absorption in nanotubes

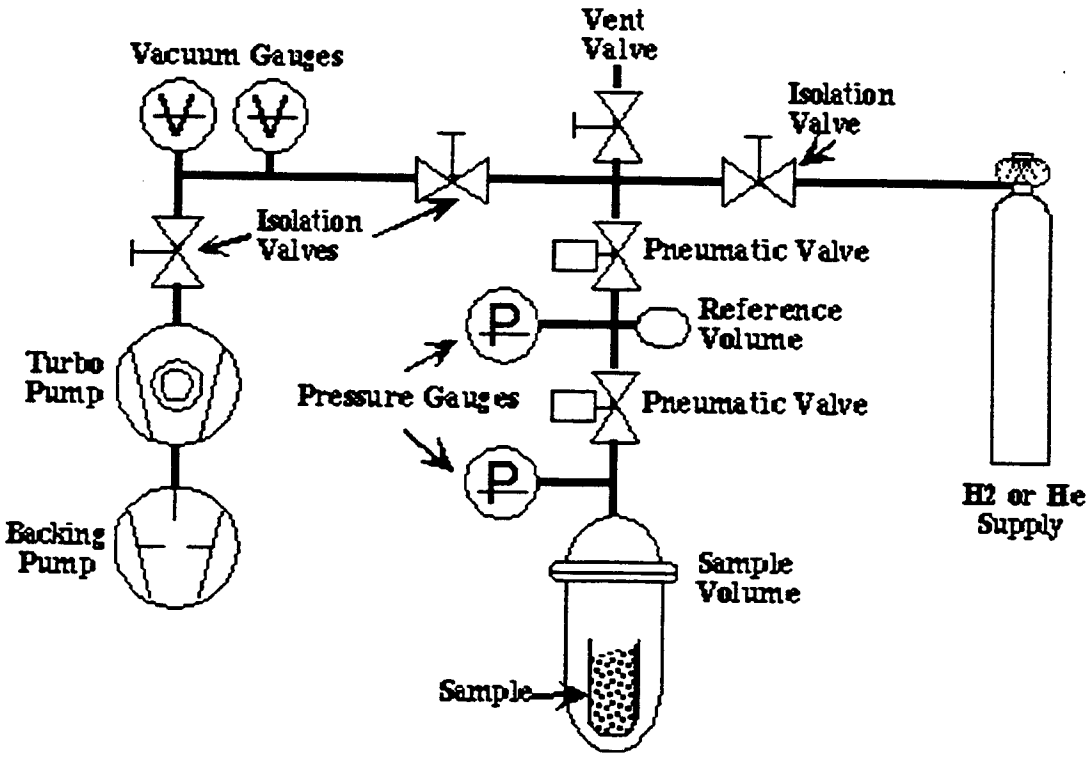

Figure 7